https://doi.org/10.3311/PPme.14176
Creative Commons Attribution

Periodica Polytechnica Mechanical Engineering, 64(1), pp. 31–42, 2020

Fluid Thermal Effect on Non-contacting Labyrinth Seal of 20 MW Steam Turbine

Lahouari Mammar[1], Yahiaoui Tayeb[1], Omar Ladjedel[2], Ondřej Šikula[2*]

[1] Laboratoire d'Aéronautique et Systèmes Propulsive, Département de Génie Mécanique, Université des Sciences et de la Technologie d'Oran Mohamed-Boudiaf El Mnaouar, P.O.B. 1505, Bir El Djir 31000, Oran, Algérie
[2] Institute of Building Services, Faculty of Civil Engineering, Brno University of Technology, Brno 60200, Veveří 331/95, Czech Republic
* Corresponding author, e-mail: sikula.o@vutbr.cz

Received: 09 April 2019, Accepted: 29 October 2019, Published online: 17 December 2019

Abstract

This paper is divided into two parts; the first describes a CFD analysis of a gland packing labyrinth seals in 20 MW steam turbine in LNG plant using ANSYS CFX code as an isothermal simulation in fluid domain. The results of two turbulence models k-ε and k-ω SST are compared and validated against experimental data. It is shown that the labyrinth seal leakage is proportional to the clearance cube so any variation in clearance can have a significant impact on the steam leakage. This clearance between the shaft and the labyrinth seal vary as a function of operating temperature due to the different rates of thermal expansion of the materials for these two components. Likewise the fluid temperature has a direct effect on fluid dynamic behavior. For that; the second part of the paper investigates the effect of fluid thermal conditions of the labyrinth seal via the heat transfer and Nusselt number variation in the stator and the rotor, for different cases of inlet temperature (400 °C, 200 °C, 100 °C, 50 °C) and pressure ratio (2.5, 4.5, 6.5) for an ideal gas. Also it is important to know the temperature distribution across tooth and cavities of the labyrinth seal, and finally the Influence of Inlet total temperature on fluid pressure drop in the labyrinth seal will be treated for improving and readjusting the steam turbine sealing system.

Keywords

labyrinth seals, heat transfer, CFD analyses, steam turbine, turbomachinery

1 Introduction

High pressure side and low pressure side of the turbine casing, where turbine rotor extrude the casing, must be sealed against of air and steam leakage using glands labyrinth seals. The 396 mm shaft diameter of the studied steam turbine has a Labyrinths dependent upon radial clearances design of 0.4 mm to 0.5 mm with "high and low" teeth, thin teeth are part of the turbine shaft (8 mm for the low teeth and 12 mm for the high), and heavy teeth (cavity with 4 mm deep and 4.5 mm large) are cut on the renewable packing ring which is made in segments backed and held inward by a springs system.

Experimental labyrinth seal research began to shift from trying to gain a better understanding of the labyrinth flow field to searching for ways to optimize labyrinth seal performance. The potential for development in labyrinth seals performance for high pressure ratio gas turbines have been discussed by Stocker [1], however a comparison with data derived from detailed measurements in test facility are reported by Wittig et al. [2]. Although the leakage flow through labyrinth seals under stationary and rotating conditions has been examined by El-Gamal et al. [3]. Sriti et al. [4] investigated the purpose of controlling better the flows within the labyrinth seals and to determine their static (leakage-pressure) and dynamic (stiffness and damping coefficients) characteristics.

Both computational fluid dynamics (CFD) and an analytical tool were used to predict the leakage flow of different seal configurations with various clearances in Kim and Cha [5] modulation. Zhao et al. [6] analyzed the influence of the cavity on the leakage behavior of labyrinth seals in the aim to develop an optimum design. An example of such an effort can be seen in the shape optimization work of Schramm et al. [7]. Also the influence of the boundary conditions on labyrinth rotordynamic instability was investigated by Xi [8].

The fundamentals for describing the flow through straight labyrinth seal equations are presented in Saikishan [9] study.

Cite this article as: Mammar, L., Tayeb, Y., Ladjedel, O., Šikula, O. "Fluid Thermal Effect on Non-contacting Labyrinth Seal of 20 MW Steam Turbine", Periodica Polytechnica Mechanical Engineering, 64(1), pp. 31–42, 2020. https://doi.org/10.3311/PPme.14176

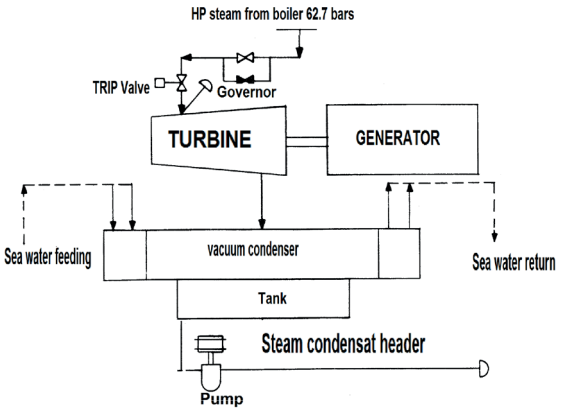

Fig. 1 Simplified diagram of the turbine installation.

Hiester [10] summarized the seal convection heat transfer characterization where heat transfer coefficients are calculated with and without viscous heating. The previous studies were very helpful to determine methods of the rational choice of a labyrinth seal design for gas pumping units by Bellaouar et al. [11] and to investigate new designs and geometries as the trapezoidal teeth labyrinth seal by Abdous and Zirak [12].

The subject turbine of this paper is a total condensation steam turbine. The steam at 62.7 bar and 440C expand through the turbine and then condensed in a vacuum condenser at 101 mmHgA (Fig. 1). Within 15 stages, this turbine contains a 20 MW shaft power turning at 3000 rpm.

1.1 Turbine sealing system description

Metallic labyrinth packing subject of this paper are employed to reduce internal steam leakage from escaping the turbine from elevated-pressure ends, and prevent air from leaking into the turbine at sub atmospheric-pressure shaft ends.

Steam leaked from high pressure side of the casing is led to the lower pressure stage after passing through the first labyrinth gland (Fig. 2).

Leakage from the second gland and spindle of governor valves is collected in the gland steam receiver of which pressure is regulated by a pressure control valve at 1.05 to 1.1 bar and from which sealing steam for lower pressure is supplied.

The number of labyrinth of each gland is so designed that the lower pressure side gland can be sealed by the leakage from the high pressure side gland and no auxiliary steam supply is necessary at normal load operation.

Outer leakage from the turbine shall be collected by a gland condenser which has a slightly lower pressure than the atmosphere pressure by a vapor extractor. Thus steam leakage to atmosphere can be avoided.

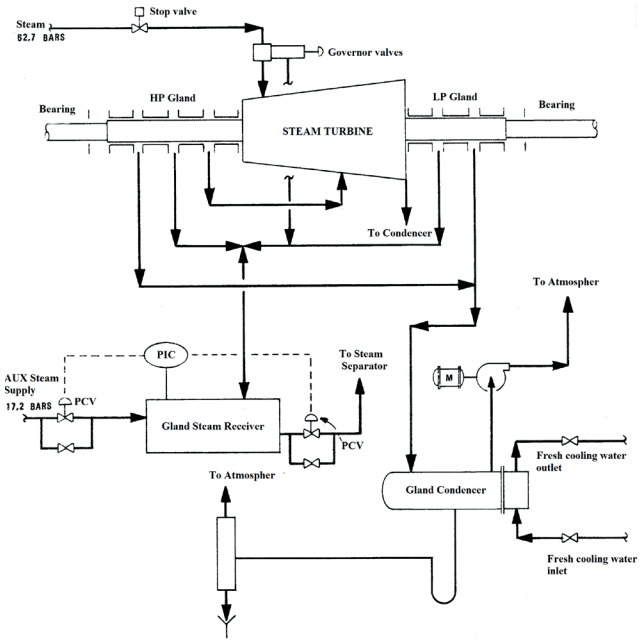

Fig. 2 Schematic diagram of the gland seal system.

1.2 Glands technology description

The gland bushes which are split horizontally and equipped with metal packing rings inserted in the T grooves of bushes are provided for the high and low pressure ends of casing to compose of glands (Fig. 3).

The narrow clearances between metal packing rings which are divided into eight pieces and keep their position correct by plate type springs, and labyrinth fins which are provided on turbine rotor, serve to prevent the steam from leaking off and air from entering into the casing (Fig. 4).

The HP and LP glands are composed of four and three sections respectively (Fig. 5). A majority of leakage steam from HP turbine casing is sent to LP stage through No.4

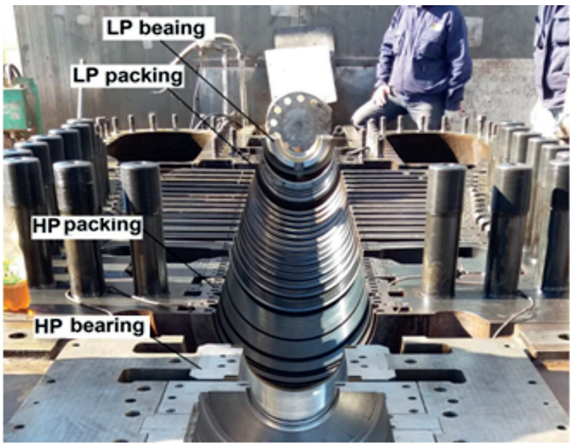

Fig. 3 20MW, 15 stages, condensing steam turbine with dismounted rotor [13].

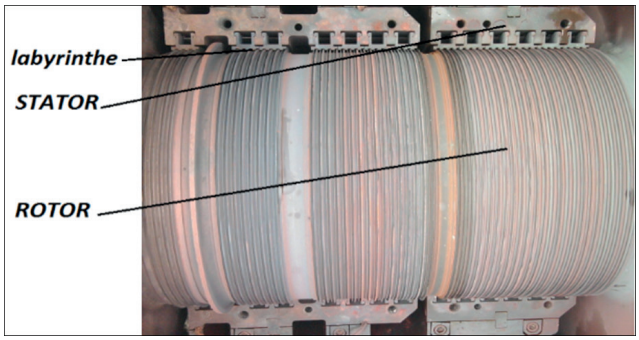

(a)

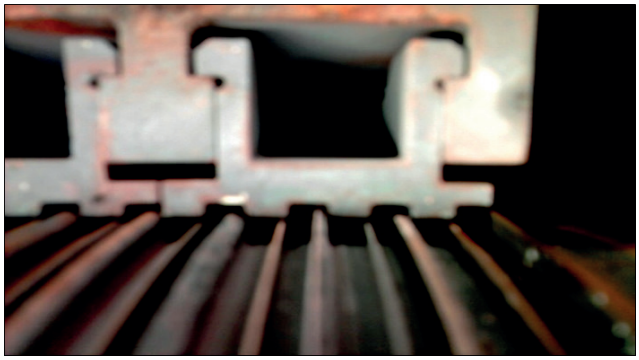

(b)

Fig. 4 (a) HP side gland packing, (b) thin teeth, and heavy teeth of packing [13].

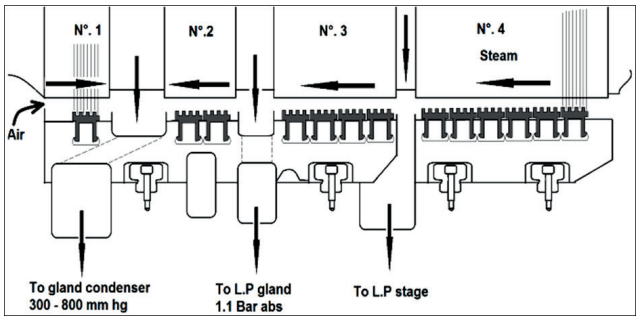

Fig. 5 High pressure side gland with blocks disposition.

block and then the rest steam through No.3 block is led to LP gland being kept at 1.1 bar. by abs pressure control valves for prevent of air invasion into exhaust casing.

The leakage steam through No.2 block of HP and LP side gland are led to gland condenser with air leakage from external by means of a vapor extractor to prevent external gland leakage and possible contamination of bearing oil Fig. 5.

Labyrinth seals also have high steam leakage rates that can damage bearings and other components. Field experience shows that even under the best of circumstances. Temperature differences and cyclic variations in at between vent areas and ambient promote condensation. The possibility of ingesting wet or contaminated air exists also at the shaft seals. Large amounts of oil draining from the bearing area back to the reservoir are known to create suction effects or slightly lower pressure regions in the bearing housing. This promotes the inflow of ambient air mixed with height temperature steam from HP leakage packing through labyrinth seals and condensation in oil reservoirs. A centrifugal oil purifier is almost permanently connected to the oil reservoir to prevent lubricating and regulation oil from contamination.

The aim of this study is to investigate the fluid temperature effect on the performance of non-contacting labyrinth seal of steam turbine. A Numerical approach is used for flow analyzes and comparison between several cases. The simulations were performed by using the ANSYS CFX software.

2 The CFD solver

The CFD code used in this work is Ansys CFX and is based on a finite volume method which uses an unstructured mesh containing hexahedral and prism elements. This has the advantage that local numerical diffusion is reduced and is therefore suitable for complex flows with reversal flow.

The code is based on a coupled solver for solving the differential equations using the fully implicit discretization method and treating the hydrodynamic equations as one single system. To reduce the number of iterations required for convergence, a false-time stepping method is imposed which guides the approximate solutions in a physically based manner to a steady-state solution [14].

Buoyancy is modeled using the Boussinesq approximation in which the forces are modeled as source terms in the momentum equations. In this study, two turbulence models k-ε (Patankar and Spalding [14]) and k-ω SST (Menter [16]) are used for the turbulence modeling. Compared to the commonly used k-ε turbulence model, the k-ω model implies a new formulation for the near wall treatment which provides an automatic switch from a wall-function to a low-Reynolds number formulation based on the near-wall grid spacing. This makes it more accurate and more robust. The turbulence viscosity is assumed to be linked to the turbulence kinetic energy (k-equation) and turbulent frequency (ω-equation) instead of the turbulence dissipation rate (ε-equation in the k-ε model). To overcome the sensitivity of the k-ω model to freestream conditions, the SST model was developed. It blends the k-ω model near the surface with the k-ε model in the outer region. To predict correctly the near wall flow, a mesh resolution is set to give a value of y^+ under two in the cas of the k-ω SST model, and a value between 20 and 100 in the cas of k-ε model.

2.1 Consideration Y⁺Plus

As described by the Solver Theory [14], it is important to note that to fully resolve the boundary layer, you should put at least 10 nodes into the boundary layer as shown in Fig. 6. (a) (Mesh illustration).

The upper limit for y^+ is a function of the device Reynolds number. For example, a large model may have a considerable Reynolds number and y^+ can safely go to values much greater than thousands. For lower Reynolds numbers, the entire boundary layer might only extend to hundreds. In this case, a fine near wall spacing is required to ensure a sufficient number of nodes in the boundary layer.

2.2 Validation of the numerical model

While CFD solver sometimes does not give very accurate predictions of overall aerodynamic performance, it at least shows local flow fields and relative performance comparisons between different configurations and allows adjusting the CFD SOLVER parameters.

Predicted leakage behaviors according to clearance size and pressure ratio were compared with experimental data for the validation of the numerical model before studying the objects cases of this paper.

Details of the experimental facility are presented elsewhere [16, 17] and only a short description is included here. A schematic of the experimental test rig is shown in Fig. 7.

Air is supplied by a compressor with a maximum mass flow of 0.5 kg/s and maximum pressure ratio of 4. The supply pressure is kept constant at about 3.5 bar by means of a bypass valve. The determination of the mass flow rate is accomplished by one of three parallel orifice meters which are connected to a precision water pressure gauge. The mean flow rate is controlled by valves behind the orifice meter section. The electric heater is designed for a maximum exit temperature of 400 °C. A settling chamber serves to obtain an even velocity profile in front of the test section. The labyrinth seal in the test section consists of an upper part either with or without steps (stator) and a lower part with fins (rotor). Both parts are assembled with spacers to allow adjustment of the gap widths.

Fig. 8 identifies the geometry of the labyrinth forms under investigation. The parameter variation is illustrated in Table 1.

Table 1 Labyrinth seal geometric variables

Seal type	Ns	s (mm)	t (mm)	b (mm)	h (mm)
Straight-through	6	0.5 - 2.5	12	2.5	10.5

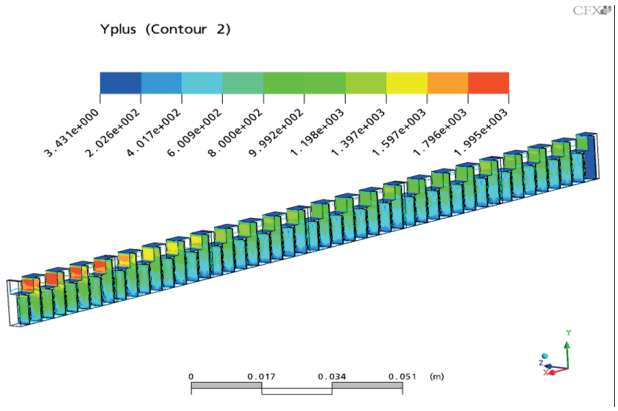

Fig. 6 Y⁺ contour in the stator

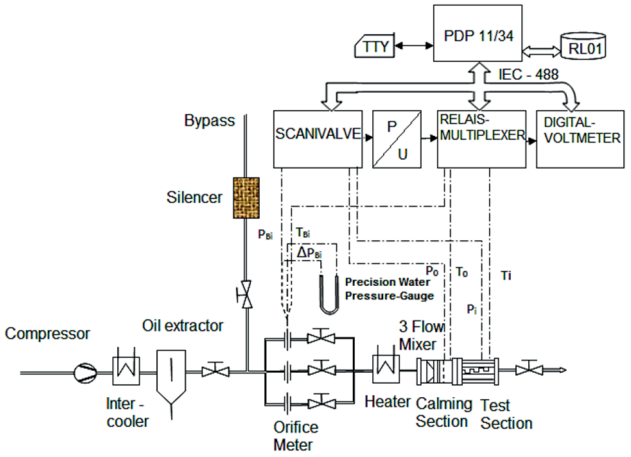

Fig. 7 Labyrinth seal test facility.

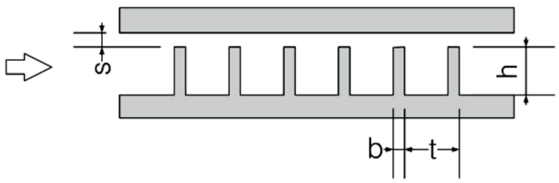

Fig. 8 Labyrinth seal geometry.

The pressure distribution in the labyrinth chamber is very uniform except along the most upper part of the fin. Depending on the gap width, the flow contraction behind the first fin may cause a pressure rise in the second chamber which leads to a relative pressure minimum in the first chamber, as shown by Wittig et al. [18, 19].

The Pressure difference is defined as follow:

$$\xi = 1 - \frac{\Delta P}{\Delta P_{\max}}, \tag{1}$$

Where $\Delta P_{\max} = P_0 - P_\infty$, $\Delta P = P_0 - P_n$, P_0 is the pressure in the settling chamber. P_∞ is the pressure behind labyrinth. P_n is the pressure behind the specified n fin.

The pressure drop is shown in Fig. 9. In Fig. 10 the numerical results are compared with the experimental ones. The Ansys CFX results show the same uniformity pressure distribution in the labyrinth chamber as described before. There is to mention that a significant pressure rise is noted for N°3 as shown in Fig. 10 (d) in both compared experimental and CFD results. This pressure rise is proportional to the pressure ratio rise.

Also the Ansys CFX velocity field for the straight seal is compared with a valid CFD model STAR-CCM+, [5] the calculated velocity field of labyrinth [2]. As shown in Fig. 11, the velocity field of the six-fin straight-through labyrinth, is described by vector presentation and by lines of constant velocity. The recirculation regions in the individual chambers for the ANSYS CFX are located similar as the valid calculated velocity field [2]. However, the CFD model STAR-CCM+, [5] present a slight coincidence with the center of the cavity instead of the right side.

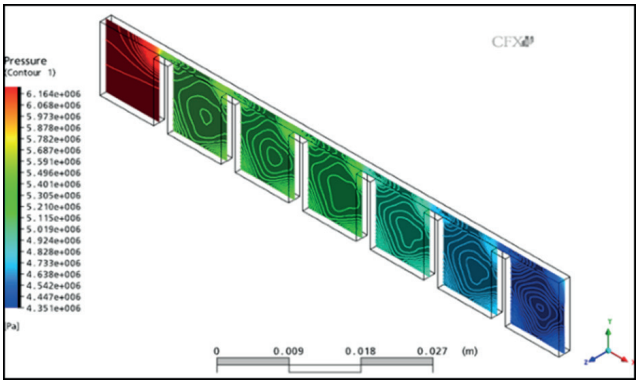

Fig. 9 Pressure Distribution in the straight seal Ansys CFX validation model.

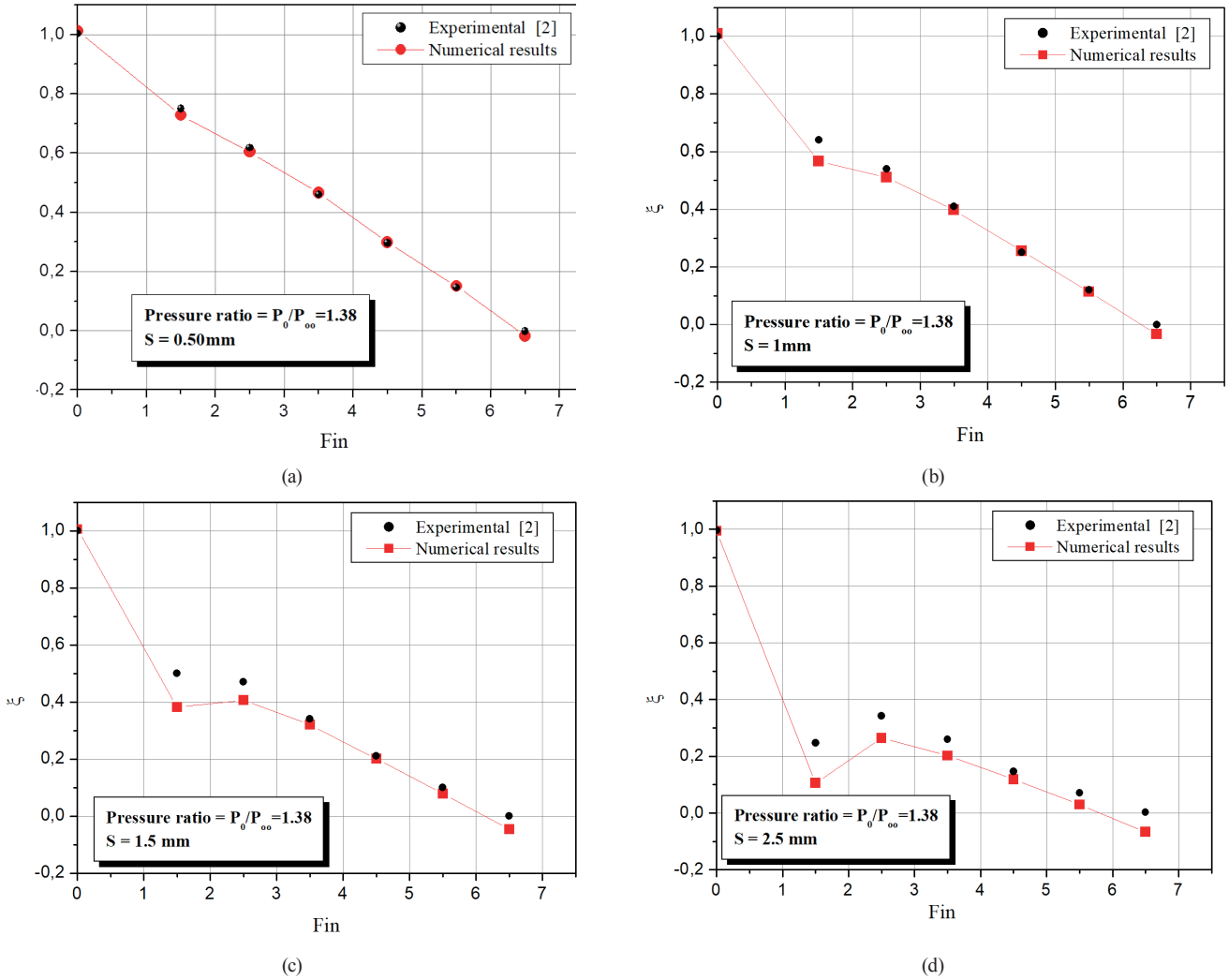

Fig. 10 ANSYS CFX Pressure Distribution results comparison with the experimental data in the straight seal.

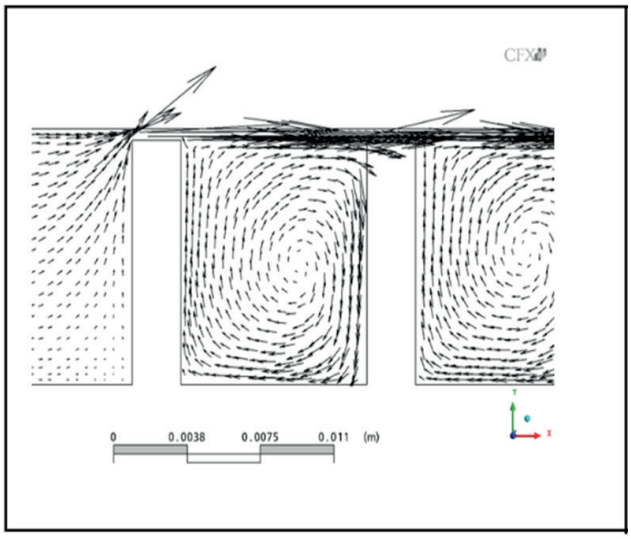

(a)

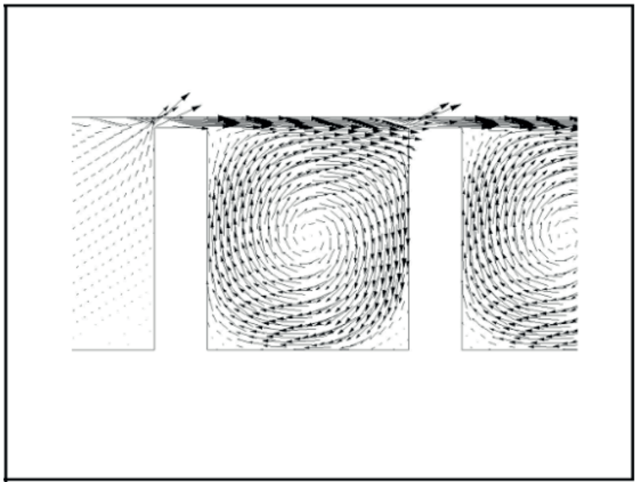

(b)

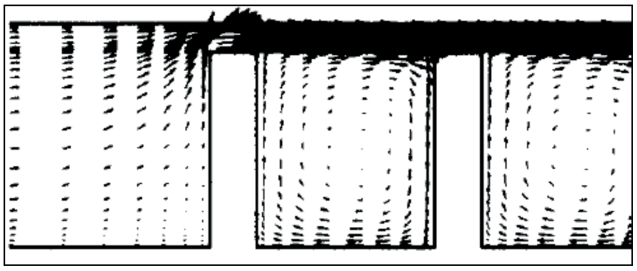

(c)

Fig. 11 Velocity field for the straight seal with a clearance of 0.5 mm. (a): Academic Ansys CFX code; (b) commercial finite volume code, STAR-CCM+ [5] and (c) calculated velocity field of Wittig et al. [2].

2.3 Numerical models

The geometry and boundary conditions of the fluid model are based on data and parameters of 20MW, 15 stages, condensing steam turbine driving electrical power generating for LNG plant Fig. 12.

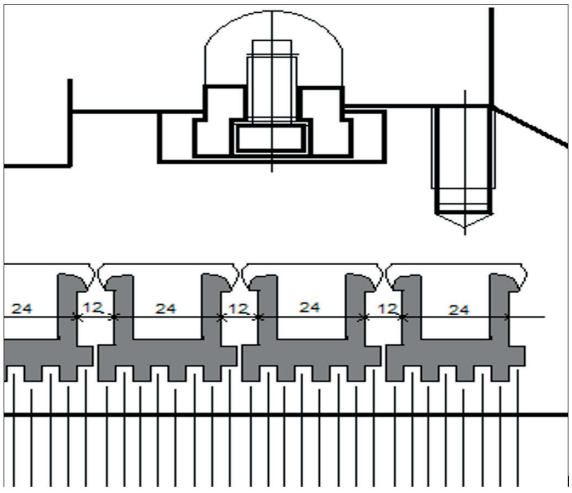

(a)

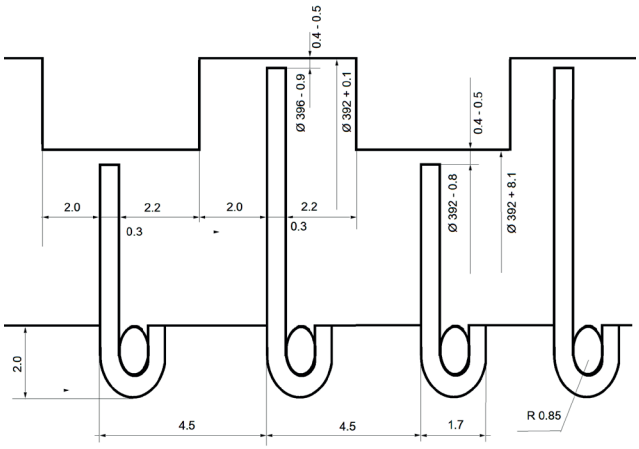

(b)

Fig. 12 20MW steam turbine sealing details: (a) gland system, (b) fins and cavity details.

The working fluid is dry steam at 440 °C for the first case and compressible air governed by ideal gas law for the second case. The inlet total temperature is set at working and cases studies temperatures. Inlet total pressure is set at working pressure and outlet static pressures are varied to yield various pressure ratios. The validity of the standard k-ε turbulence model used here for straight–through labyrinth seals has been repeatedly demonstrated in references. The mesh density and the near–wall element size are verified, resulting in several cases of mesh since 480.000 to 1.4 million hexahedral elements Fig. 13.

In order to approach the real profile of inlet static pressure distribution to set in the inlet boundary condition of the labyrinth, we proceed to modeling a CANAL using k-ε model in ANSYS-CFX where the inlet static pressure is set at 62 bars and the result of the pressure distribution near the outlet CANAL Fig. 14 is saved in DATA as

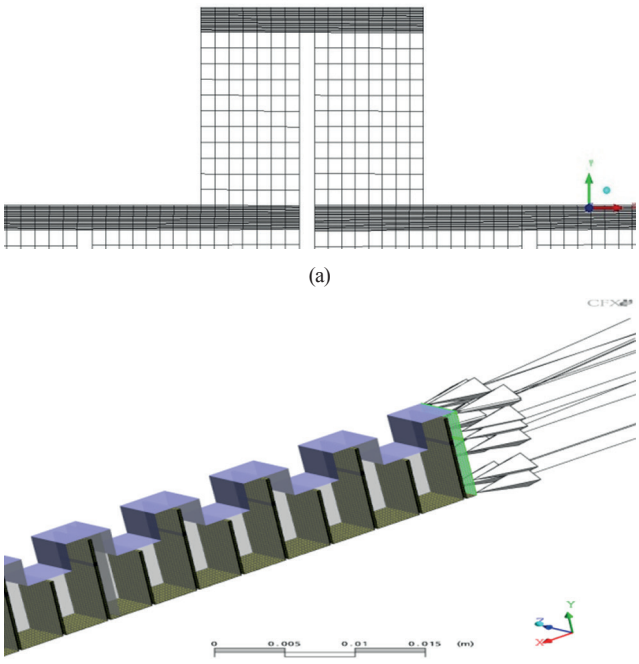

Fig. 13 (a) Mesh illustration, (b) Fluid model of the labyrinth seal (mm)

input condition for inlet boundary condition in the labyrinth simulation.

2.4 Boundary conditions

The imposed boundary conditions are as follows (Fig. 15):

- Inlet total temperature = 400 °C
- Inlet pressure: 62 bar.
- Outlet pressure: 09 bar.
- Boundary interface: symmetry
- Shaft velocity: rotating 3000 rpm.

3 Results and discussions

3.1 Case 01: Isothermal model

In this case heat transfer at walls can be neglected, thus the stator and the rotor are modeled as adiabatic walls, which is a common practice in CFD simulations of labyrinth seals. Detailed flow features are presented as follow.

3.1.1 Stream lines velocity

Fig. 16 shows that a large vortex between the two teeth can be recognized. Above the vortex, there are a major and a secondary recirculation zones behind and in front of the cavity, respectively.

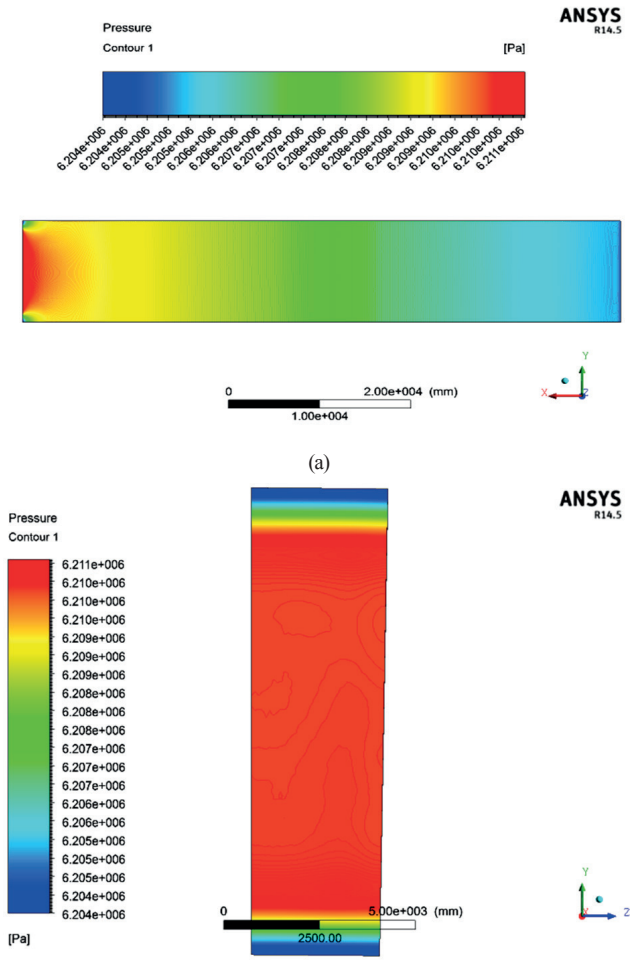

Fig. 14 Static pressure distribution, (a) along the canal, (b) at the outlet plane.

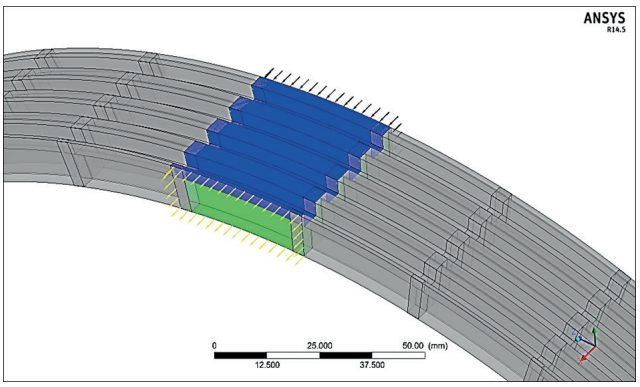

Fig. 15 Boundary conditions.

3.1.2 Static pressure

It is found in Fig. 17 that static pressure decreases along the flow direction and varies very little within each cavity.

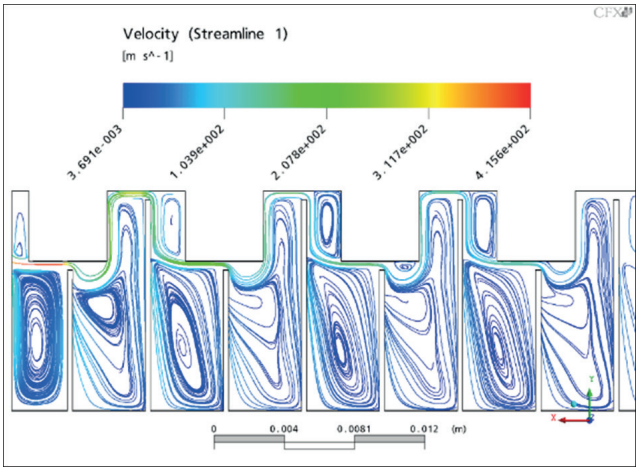

Fig. 16 Streamlines in labyrinth seal, packing N°06.

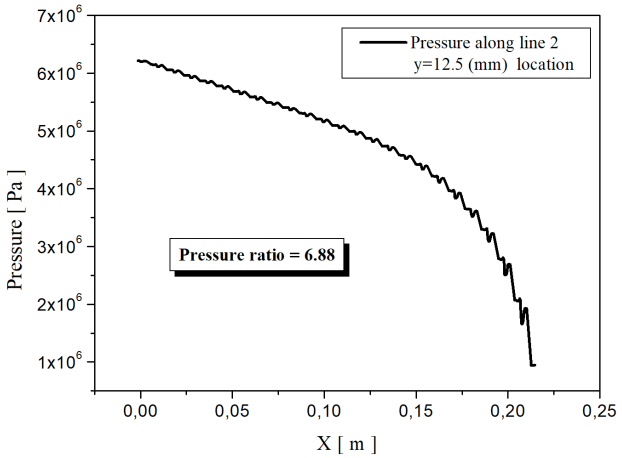

Fig. 17 Pressure along the labyrinth seal for all the six packing.

3.1.3 Turbulent models and grids sizes comparison

A comparison of the results obtained by means of the ANSYS CFX in Fig. 18. Numerical analyses were conducted for the same boundary conditions and the analysis has shown that the results obtained are very similar.

3.2 Case 02: Total energie model

The thermal effects of a high temperature labyrinth seal are investigated. This case focuses on CFD and Heat transfer behavior across the labyrinth seal and no mechanical and thermal fluid structure interaction including the thermal expansion are developed. Detailed flow features are presented as follow.

3.2.1 Circumferential velocity

Fig. 19 shows that the circumferential velocity increases from zero along the walls to its maximum values at the end of each tooth of the rotor fins.

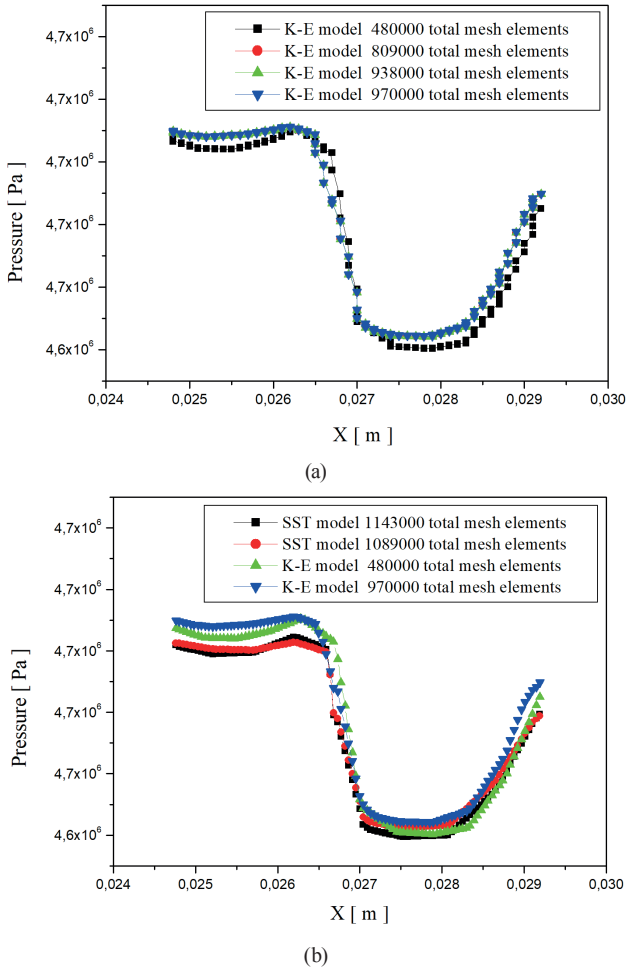

Fig. 18 (a) Grid sizes comparison, (b) Turbulence models comparison

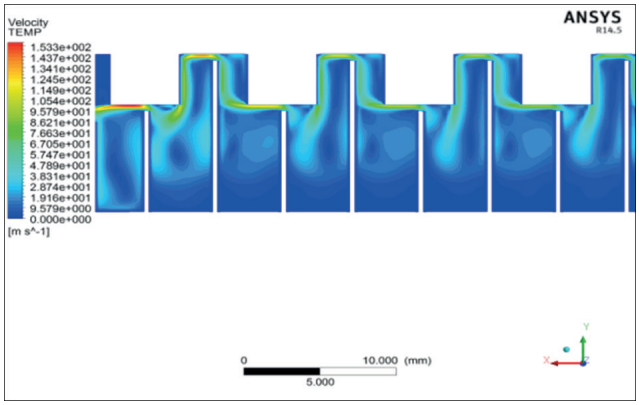

Fig. 19 Velocity contour in the last seal cartridge.

3.2.2 Static temperature

The static temperature is raised across the seal, which is mainly due to friction at the rotating wall (Fig. 20). This slight temperature rise can be noted for the fourth cases inlet temperature studied. However the drop temperature caused by the pressure drop in the cavity is very significant.

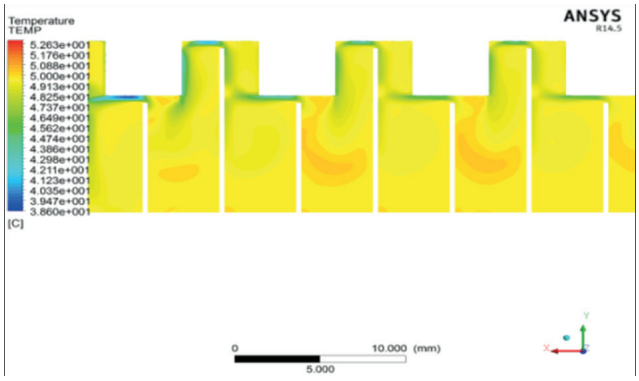

(a)

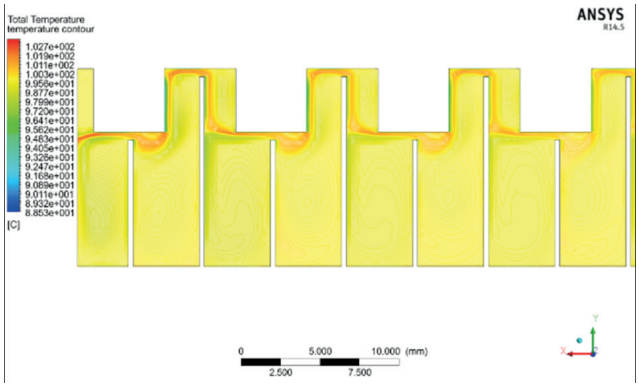

(b)

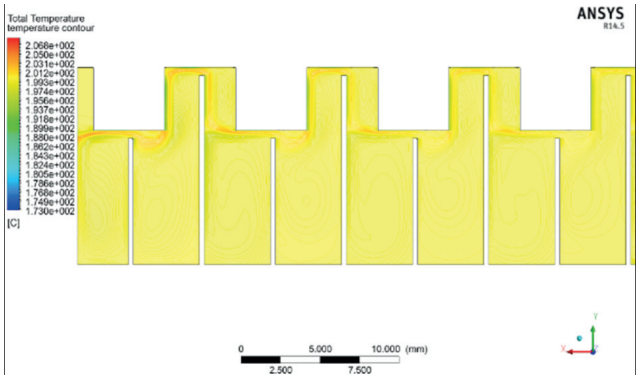

(c)

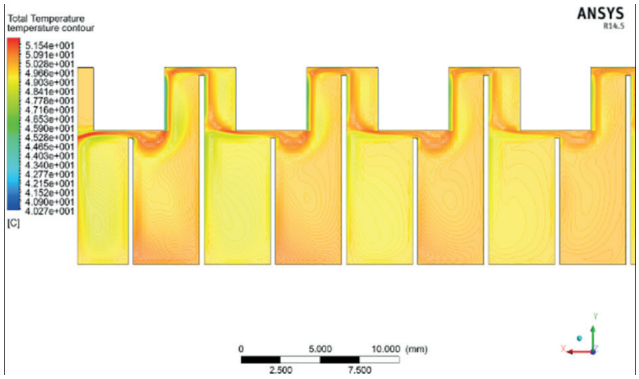

(d)

Fig. 20 Temperature contour: (a) inlet temperature 50 °C; (b) inlet temperature 100 °C; (c) inlet temperature 200 °C; (d) inlet temperature 400 °C

3.2.3 Static pressure

The pressure distribution of the entire model is shown in Fig. 21. It is shown that each labyrinth tooth creates a pressure drop.

3.2.4 Wall heat transfer coefficient

The wall heat transfer coefficient increases along the labyrinth as shown in the contour plot in the stator wall in Fig. 22.

3.2.5 Temperature distribution across the labyrinth seal

In Fig. 23, the temperature distribution is demonstrated. There are clear temperature peaks at the tooth tips than the peak values decrease from the second tooth to the fourth tooth.

3.2.6 Mean Nusselt number of the rotor and the stator

In Fig. 24 and Fig. 25, the mean Nusselt number is computed and compared using CFD ANSYS CFX model for the stator and rotor surfaces. The mean Nusselt numbers are studied in terms of the pressure ratio, and inlet total temperature as the work of Du and Schäfer [19]. Generally, high pressure ratio leads to high Reynolds number and hence high Nusselt number, suggesting more heat is transferred from the hot air to the surface. High inlet total

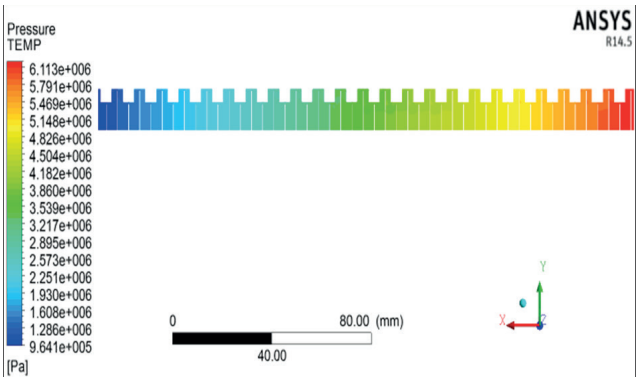

Fig. 21 Static pressure along the labyrinth seal.

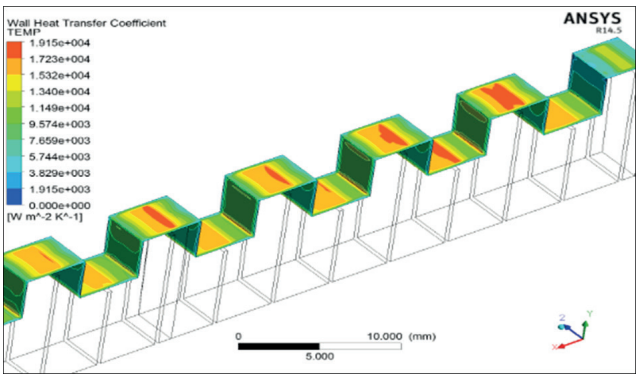

Fig. 22 Wall heat transfer coefficient contour in the stator

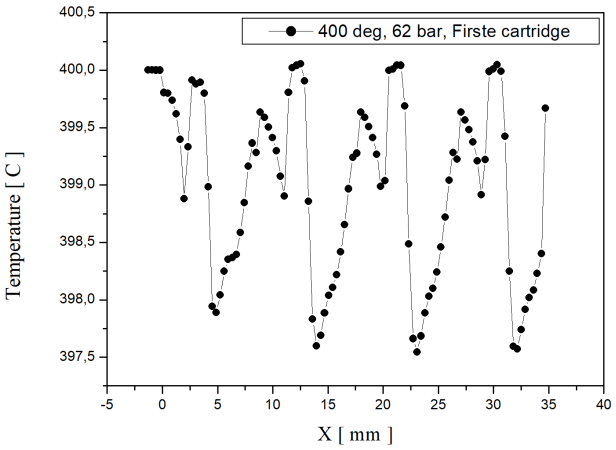

Fig. 23 Temperature distribution along the labyrinth seal.

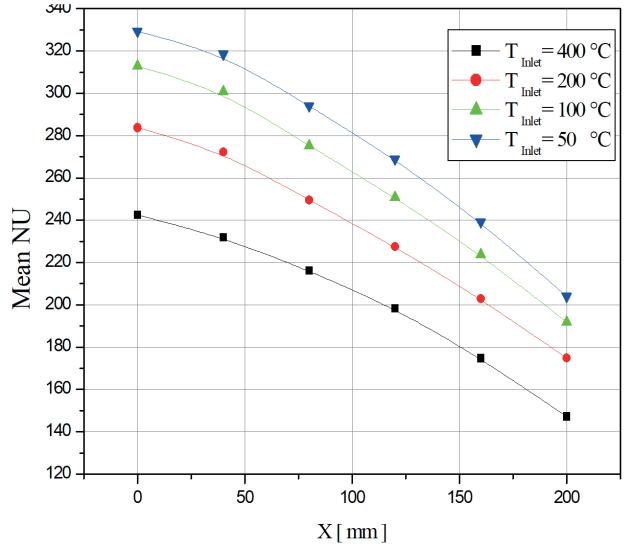

(a)

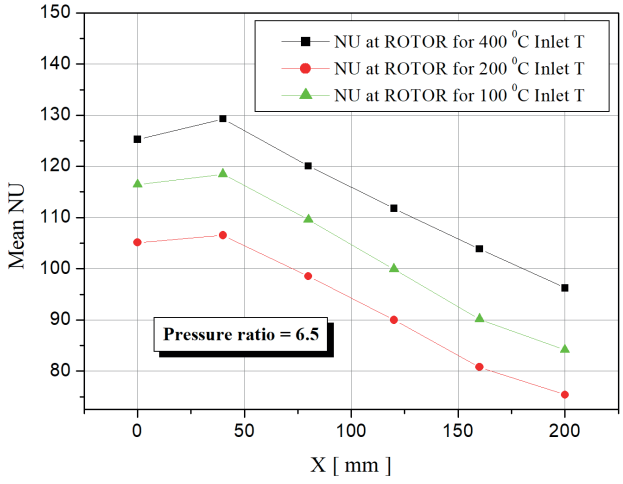

(b)

Fig. 24 Mean Nusselt number for pressure ratio = 6.5; (a) stator; (b) rotor.

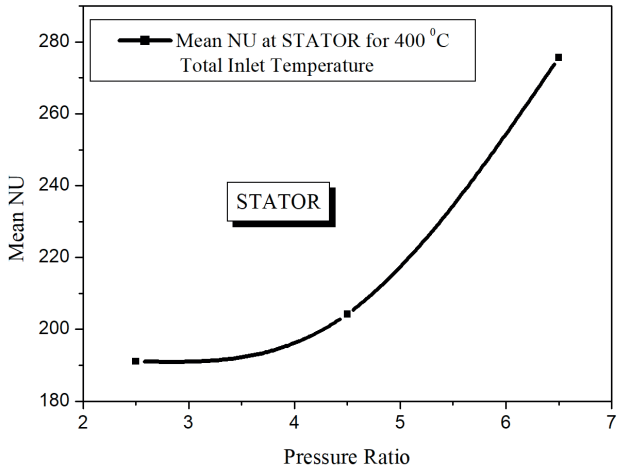

(a)

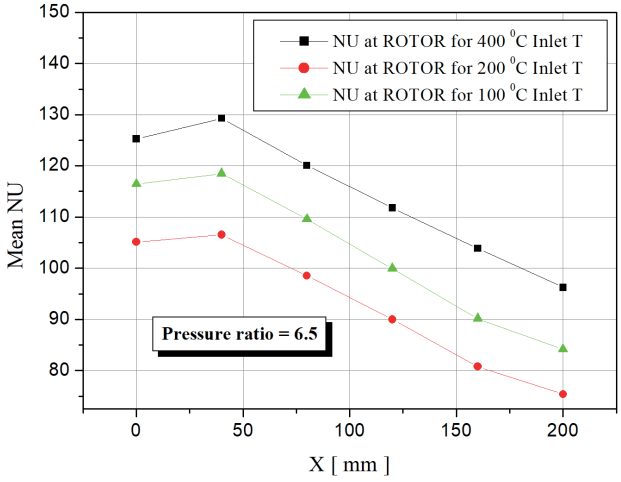

(b)

Fig. 25 Mean Nusselt number for inlet temperature= 400°C; (a) stator; (b) rotor

temperature results in high rotor and stator surface temperatures as expected. However, the inlet total temperature influences the heat transfer across the fluid–surface boundaries. Growing the inlet total temperature leads to a slight decrease of the Nu number. To be noticed that for the same pressure ratio, NU number decrease about 11 % for each 50 °C inlet total temperature rises.

3.2.7 Influence of inlet total temperature on pressure drop in labyrinth seal

Fig. 26 illustrates the pressure across the labyrinth seal for the first cartridge and the third one under 6.5 pressure ratio. The influence of the inlet total temperature is very distinctive comparing pressure distribution for 400 °C inlet total temperature with 50 °C and 100 °C inlet total temperature, where the difference could reach 0.3 bar at

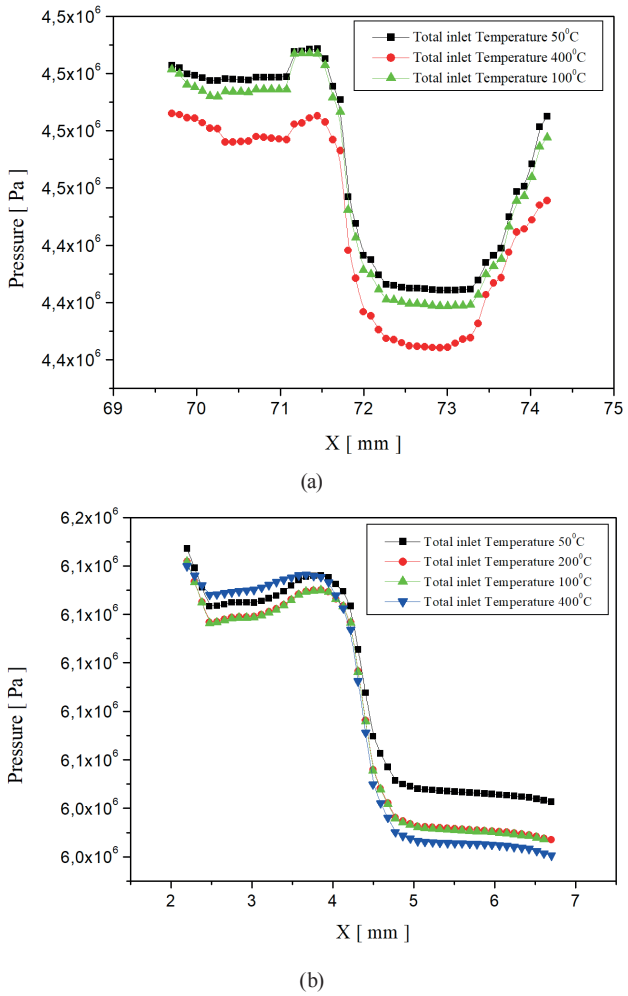

Fig. 26 Pressure across the labyrinth seal for pressure ratio = 6.5; (a) cavity cartridge N° 01; (b) knife cartridge N° 03.

long fin and 0.5 bar at short fin. However the pressure difference is negligible comparing fluid at 100 °C and 200 °C.

4 Conclusion

This paper presents a numerical prediction of the flow through a labyrinth seals. The ANSYS-CFX code is used to solve the highly three dimensional viscous flow. The computed pressure drop is in reasonable agreement with experimental data.

After the ANSYS CFX validation by experimental comparison, the first case treated as no heat transfer at walls, thus the stator and the rotor are modeled as adiabatic walls, and in this case the results of several computational grids are compared using two turbulence models k-ω SST model and k-ε model.

The second case focuses on the thermal effect phenomenon on labyrinth seal, several results were computed as, static temperature and pressure distribution, mean Nusselt number of the rotor and the stator, influence of inlet total temperature on pressure drop.

Even if the influence of the inlet total temperature appears insignificant (0.3 bar at long fin and 0.5 bar at short fin) comparing pressure at 400 °C inlet total temperature with 50 °C and 100 °C inlet total temperature, it will have a very significant impact on leakage control system described before in the Turbine sealing system paragraph where pressure is controlled in the gland steam receiver by a pressure control valves set at 1.05 to 1.1 bar and any perturbation on pressure will rise the consumption of the auxiliary steam (17.2 bar) or venting the steam at the atmosphere. These results enhance our understanding of the thermal effects in labyrinth seals.

Acknowledgment

Research was supported by Specific research at Brno University of Technology; project FAST-J-19-5976.

Nomenclature

b	fin width	[M]
h	fin height	[M]
P	pressure	[Pa]
P_0	pressure in the settling chamber	[Pa]
P_∞	pressure behind labyrinth	[Pa]
P_n	pressure behind the specified N fin	[Pa]
s	gap width	[M]
t	pitch	[M]
T	temperature	[°C]
V	velocity	[M.S^{-1}]
X	length coordinate	[M]
ΔP	pressure difference	[Pa]
ΔP_{max}	maximum pressure difference	[Pa]
N_s	number of fin	[-]
NU	Nusselt number	[-]
ξ	pressure coefficient	[-]

References

[1] Stocker, H. L. "Advanced Labyrinth Seal Design Performance for High Pressure Ratio Gas Turbines", In: ASME 1975 Winter Annual Meeting: GT Papers, Houston, TX, USA, Paper number: ASME 75-WA/GT, V001T01A005.
https://doi.org/10.1115/75-WA/GT-22

[2] Wittig, S., Schelling, U., Kim, S., Jacobsen, K. "Numerical Predictions and Measurements of Discharge Coefficients in Labyrinth Seals", In: ASME 1987 International Gas Turbine Conference and Exhibition, Anaheim, CA, USA, 1987, Paper number: 7-GT-188, V001T01A064.
https://doi.org/10.1115/87-GT-188

[3] El-Gamal, H. A., Awad, T. H, Saber, E. "Leakage from labyrinth seals under stationary and rotating conditions", Tribology International, 29(4), pp. 291–297, 1996.
https://doi.org/10.1016/0301-679X(95)00043-4

[4] Sriti, M., Agouzoul, M., Ouazar, D., Micheau, P. "Simulation numérique d'écoulement compressible dans les joints labyrinthe" (Numerical simulation of compressible flow in labyrinth seals), Journal de Physique III France, 7(5), pp. 1025–1037, 1997. (in French)
https://doi.org/10.1051/jp3:1997172

[5] Kim, T. S., Cha, K. S. "Comparative analysis of the influence of labyrinth seal configuration on leakage behavior", Journal of Mechanical Science and Technology, 23, pp. 2830-2838, 2009.
https://doi.org/10.1007/s12206-009-0733-5

[6] Zhao, W., Nielsen, T. K., Billdal, J. T. "Effects of cavity on leakage loss in straight-through labyrinth seals", IOP Conference Series: Earth and Environmental Science, 12(1), Article number: 012002, 2010.
https://doi.org/10.1088/1755-1315/12/1/012002

[7] Schramm, V., Denecke, J., Kim, S., Wittig, S. "Shape Optimization of a Labyrinth Seal Applying the Simulated Annealing Method", International Journal of Rotating Machinery, 10(5),pp. 365–371, 2004.
https://doi.org/10.1155/S1023621X04000375

[8] Xi, J. "Seal inlet disturbance boundary conditions for rotordynamic models and influence of some off-design conditions on labyrinth rotordynamic instability", PhD Thesis, Texas A&M University, 2005.

[9] Suryanarayanan, S. "Labyrinth seal leakage equation", MSc Thesis, Texas A&M University, 2009.

[10] Hiester, H. "Computational Fluid Dynamic Simulation of a Straight Labyrinth Seal", MSc Thesis, Rensselaer Polytechnic Institute Hartford, 2013.

[11] Bellaouar, A., Kopey, B. V., Abdelbaki, N. "Methods of the rational choice of a labyrinth seal design for gas pumping units", Mechanika, 19(1), pp. 81–86, 2013.
https://doi.org/10.5755/j01.mech.19.1.3611

[12] Abdous, R., Zirak, S. "Performance evaluation of trapezoidal teeth labyrinth seal", Energy Equipment and Systems, 5(3), pp. 265–273.
https://doi.org/10.22059/ees.2017.27567

[13] ANSYS Inc. "ANSYS FLUENT Theory Guide, ANSYS Help System: release 14.5", ANSYS Inc., Canonsburg, USA, 2015 [online] Available from: https://support.ansys.com/portal/site/AnsysCustomerPortal [Accessed: 25 October 2019]

[14] Patankar, S.V., Spalding, D. B. "A calculation procedure for heat, mass and momentum transfer in three-dimensional parabolic flows", International Journal of Heat and Mass Transfer, 15(10), pp. 1778–1806, 1972.
https://doi.org/10.1016/0017-9310(72)90054-3

[15] Mitsui Engineering & Shipbuilding Co., Ltd. "Corporate Action report 2015" [pdf] Available at: https://www.mes.co.jp/english/investor/reports/pdf/2015/MES_CAR2015en_all.pdf [Accessed: 25 October 2019]

[16] Menter, F. R. "Two-Equation Eddy-Viscosity Turbulence Models for Engineering Applications", AIAA Journal, 32(8), pp. 1598–1605, 1994.
https://doi.org/10.2514/3.12149

[17] Wittig, S., Kim, S., Jacobsen, K., Schelling, U. "Experimentelle und theoretische Untersuchungenzum Durchfluaverhalten und Warmeaergang in Labyrinthdichtungen" (Experimental and theoretical investigations on the flow behavior and warm aeration in labyrinth seals), VV-Abschlus Bericht, 1986. (in German)

[18] Wittig, S., Jacobsen, K., Schelling, U., Darr, L., Kim, S. "Warmeabergangszahlen in Labyrinthdichtungen" (Heat transfer coefficients in labyrinth seals), VDI-Berichte 572.1, S. 337/356, 1985. (in German)

[19] Du, Y., Schäfer, M. "Mechanical and thermal fluid structure interaction of non-contacting gas seals in jet engines", In: V. European Conference on Computational Fluid Dynamics, Lisbon, Portugal, 2010, pp. 1–14.